Carfilzomib inhibits the progression of hepatocellular cancer by upregulating GADD45α expression

MINGXUN CHEN[1,2], XU CHEN[2], YIFANG SHUI[3], CHUNYONG JI[2] and WENZHI GUO[4]

[1]Liver Transplantation Center, The First Affiliated Hospital of Zhengzhou University, Zhengzhou, Henan 450052, P.R. China; [2]Department of Hepatobiliary and Pancreatic Minimally Invasive Surgery, Zhengzhou Central Hospital Affiliated to Zhengzhou University, Zhengzhou, Henan 450052, P.R. China; [3]Department of Breast Surgery, The First Affiliated Hospital of Zhengzhou University, Zhengzhou, Henan 450052, P.R. China; [4]Department of Hepatobiliary and Pancreatic Surgery, The First Affiliated Hospital of Zhengzhou University, Zhengzhou, Henan 450052, P.R. China

Received September 20, 2024; Accepted February 6, 2025

DOI: 10.3892/ol.2025.14955

Abstract. Hepatocellular carcinoma (HCC) ranks among the most prevalent and lethal cancers affecting humans. Currently, there are limited effective treatments available for HCC. Carfilzomib, a proteasome inhibitor, is known to exert anti-HCC activities; however, its underlying mechanisms of action remain unclear. In the present study, the efficacy of carfilzomib against HCC was evaluated and its underlying mechanisms were explored. Cell Counting Kit-8, 5-ethynyl-2-deoxyuridine staining and colony formation assays were employed to analyze the antiproliferative effect of carfilzomib on MHCC-97H and Huh7 cells. Additionally, flow cytometry was used to assess the effect of carfilzomib on the cell cycle and Transwell assays were used to evaluate the effect of carfilzomib on cell migration and invasion. Western blotting was utilized to examine the protein expression levels associated with cell cycle arrest. Furthermore, short hairpin RNA (shRNA) transfection was used to investigate the role of DNA damage inducible α (GADD45α) on carfilzomib-induced cell cycle arrest. A xenograft tumor model using nude mice was employed to evaluate the anti-HCC activity of carfilzomib *in vivo*. The findings demonstrated that carfilzomib inhibited proliferation, invasion and migration in both MHCC-97H and Huh7 cells. In addition, carfilzomib caused cell cycle arrest by suppressing the expression of cyclin A2, cyclin E1 and cyclin-dependent kinases 2 and 4. Carfilzomib also upregulated the expression of GADD45α, activated the MAPK pathway and inhibited GADD45α through shRNA abolished carfilzomib-induced cell cycle arrest in HCC cells. In addition, carfilzomib inhibited Huh7 cell growth *in vivo*. To conclude, the present research revealed that carfilzomib inhibits the progression of HCC cells by upregulating GADD45α expression, suggesting that carfilzomib could be a potential chemotherapeutic agent against HCC.

Correspondence to: Professor Wenzhi Guo, Department of Hepatobiliary and Pancreatic Surgery, The First Affiliated Hospital of Zhengzhou University, 1 Jianshe East Road, Erqi, Zhengzhou, Henan 450052, P.R. China
E-mail: guowz66@163.com

Key words: hepatocellular carcinoma, carfilzomib, cell cycle arrest, growth arrest and DNA damage inducible α

Introduction

Hepatocellular carcinoma (HCC) ranks as the sixth most prevalent cancer (4.3%) and was the third leading cause of cancer-associated deaths (7.8%) worldwide in 2022, with nearly one-half of the global liver cancer cases occurring in China (1). Surgery remains the primary curative treatment for HCC; however, ~70% of patients with HCC are diagnosed at an advanced stage, rendering them ineligible for surgical resection (2). Unlike other malignant tumors, treatment options for advanced HCC are scarce, owing to its resistance to radiotherapy and conventional chemotherapy (3). Advanced-stage HCC treatments include local ablation therapy, interventional therapy, radiotherapy, chemotherapy, targeted therapy and immunotherapy. For example, the immune checkpoint inhibitors nivolumab or pembrolizumab combined with the targeted drug lenvatinib exhibited an improved tumor response compared with lenvatinib in advanced-stage HCC; however, none of the treatment effects were satisfactory in improving overall survival (4-6). Therefore, there is an urgent need for development of novel therapeutic modalities to improve clinical outcomes in patients with advanced HCC.

The introduction of proteasome inhibitors (such as bortezomib) has markedly improved the overall survival rates of patients with multiple myeloma (7). Bortezomib selectively and reversibly binds to the catalytic site of the 26S proteasome, which promotes cancer cell apoptosis (8); however, a previous study has demonstrated that bortezomib alone is ineffective in treating most solid tumors (9). Moreover, attempts to combine bortezomib with docetaxel have failed to achieve the desired clinical outcomes in advanced non-small-cell lung cancer (10). These limitations emphasize the necessity for further mechanistic research to facilitate the design of targeted therapies and improve patient outcomes.

Previous research has reported that bortezomib can induce apoptosis in HCC cells when used in combination with tumor necrosis factor-related apoptosis-inducing ligand or sorafenib (8,11,12). Furthermore, bortezomib combined with sorafenib was found to induce apoptosis in PLC/PRF/5 cells via Akt inactivation (11). The findings suggest that proteasome inhibitors may improve the therapeutic effects of sorafenib in HCC. Carfilzomib, a second-generation proteasome inhibitor, irreversibly binds to the catalytic site of the proteasome leading to prolonged inhibition (13). *In vitro* studies have demonstrated that carfilzomib exhibited superior therapeutic efficacy compared with bortezomib in multiple myeloma (14). In a rat model of diethylnitrosamine-induced hepatocarcinogenesis, carfilzomib exerted a notable preventive benefit (15). However, the efficacy of carfilzomib alone against HCC and the precise mechanisms underlying its action remain unclear.

The present study aimed to explore the efficacy of carfilzomib against the progression of HCC and investigate the underlying molecular mechanisms.

Materials and methods

Materials. Carfilzomib was obtained from MedChemExpress (cat. no. HY-10455) and dissolved in DMSO. Antibodies were procured from Proteintech Group, Inc., including cyclin-dependent kinase (CDK)2 (cat. no. 10122-1-AP), CDK4 (cat. no. 11026-1-AP), cyclin A2 (cat. no. 66391-1-Ig), cyclin E1 (cat. no. 11554-1-AP), GAPDH (cat. no. 60004-1-Ig), phosphorylated (p)-JNK (Tyr185) recombinant antibody (cat. no. 80024-1-RR), JNK monoclonal antibody (cat. no. 66210-1-Ig), p38 MAPK polyclonal antibody (cat. no. 14064-1-AP), p-p38 MAPK (Thr180/Tyr182) polyclonal antibody (cat. no. 28796-1-AP). Additionally, anti-GADD45α antibody (cat. no. A1797) was purchased from ABclonal Biotech Co., Ltd. A total of 12 4-week-old female BALB/c nude mice (15-16 g) were purchased from Beijing Vital River Laboratory Animal Technology Co.

Cell culture. MHCC-97H and Huh7 cells were acquired from Wuhan Pricella Biotechnology Co., Ltd. and cultured in Modified Eagle's medium (Gibco; Thermo Fisher Scientific, Inc.) containing 10% fetal bovine serum (Gibco; Thermo Fisher Scientific, Inc.), $1x10^5$ U/ml penicillin and 100 mg/ml streptomycin (Beijing Solarbio Science & Technology Co., Ltd.) in a constant temperature incubator at 37˚C and 5% CO_2. Cells were treated with different concentrations of carfilzomib and control cells treated with the same concentration of DMSO.

Cell viability assay. The cytotoxic effects of carfilzomib on MHCC-97H and Huh7 cells were assessed using Cell Counting Kit-8 (CCK-8; Beyotime Institute of Biotechnology). Cells were cultured in 96-well plates ($3x10^4$ cells/well) and subsequently treated with different concentrations of carfilzomib or DMSO (0, 10, 20, 30, 40, 50, 60, 80 and 100 μM) for 24 h at 37˚C. Following treatment, 10 μl CCK-8 solution was added to each well and incubated for an additional 1 h at 37˚C. Absorbance was measured at 450 nm using a Multiskan FC microplate reader (Thermo Fisher Scientific, Inc.) (16).

Cell proliferation assay. The evaluation of MHCC-97H and Huh7 cell proliferation was performed using an 5-ethynyl-2-deoxyuridine (EdU) staining kit (Beyotime Institute of Biotechnology) following the manufacturer's instructions (17). Briefly, 5,000 cells were cultured into a 96-well plate. The following day, the cells were treated with carfilzomib (30 μM for MHCC-97H cells and 60 μM for Huh7 cells) at 37˚C for 24 h. For the EdU staining assay, each well was treated with 10 μM EdU working solution and was incubated for 2 h at 37˚C. The nuclei were stained with DAPI for 10 min at room temperature and EdU-positive cells were visualized using a fluorescence microscope (Olympus Corporation). ImageJ software (version 1.51, National Institutes of Health) was used for sample analysis.

Colony formation assay. MHCC-97H and Huh7 cells were seeded in 6-well plates ($1x10^4$ cells/well) and incubated for 24 h at 37˚C. Subsequently, the cells were treated with carfilzomib (30 μM for MHCC-97H cells and 60 μM for Huh7 cells) at 37˚C and cultured for 14 days. The culture medium containing carfilzomib was replaced every 3 days throughout this period. Colonies were washed with PBS, fixed with 4% paraformaldehyde at room temperature for 10 min and crystal violet (0.1%) was then used to stain the colonies at room temperature for 20 min (18). After washing, colony formation was observed using an inverted light microscope. Colonies consisting of ≥50 cells were counted. ImageJ software (version 1.51; National Institutes of Health) was used for data analysis.

Transwell migration and invasion assays. Cell migration and invasion were assessed using Transwell chambers (pore size, 8 μm) in 24-well plates with (for invasion) or without (for migration) Matrigel (BD Biosciences). A total of 100 μl Matrigel (diluted 1:8 with serum-free DMEM medium) was added to the upper chambers of the Transwell inserts and incubated at 37˚C for 2 h before use. MHCC-97H and Huh7 cells ($1x10^5$ cells/well) were seeded in the upper chambers of the Transwell inserts with serum-free DMEM medium containing carfilzomib (30 μM for MHCC-97H cells and 60 μM for Huh7 cells). Medium containing 20% FBS was added into the lower chamber. After incubation for 24 h at 37˚C, non-migrating cells on the top of the filter were eliminated using a cotton swab. Subsequently, the migrated cells on the bottom surface of the membrane were fixed and stained with 0.1% crystal violet at room temperature for 10 min (19). After washing, attached cells were counted under an inverted light microscope. The number of cells that had migrated was counted using ImageJ software (version 1.51; National Institutes of Health).

Wound healing assays. MHCC-97H and Huh7 cells were seeded in 6-well plates at a density of $1x10^6$ cells/well until the confluency reached 90%. Subsequently, the cells were scraped with the tip of a standard 200 μl sterile pipette to create a wound and further incubated in fresh serum-free DMEM medium containing carfilzomib (30 μM for MHCC-97H cells and 60 μM for Huh7 cells) for 48 h at 37˚C. Cells were imaged with a light microscope at 0 and 48 h and the migratory capacity of the cells was assessed using the size of the healed wound area. ImageJ software (version 1.51l National

Institutes of Health) was used for data analysis. Wound closure ratio=(0 h cell migration area-48 h cell migration area)/0 h cell migration area.

Flow cytometry detection of the cell cycle. MHCC-97H and Huh7 cells were seeded in 6-well plates at a density of $5x10^5$ cells/well and treated with carfilzomib (30 μM for MHCC-97H cells and 60 μM for Huh7 cells) at 37˚C for 24 h after 12 h. After 24 h of treatment, the cells were collected and fixed in 70% ethanol at 4˚C overnight. Subsequently, the collected cells were washed with PBS, resuspended in staining buffer containing 50 μl PI and 450 μl RNase A (Beijing Solarbio Science & Technology Co., Ltd.) and incubated at room temperature for 30 min in the dark. The cells were analyzed and calculated using BD FACSCanto™ Flow Cytometer (BD Biosciences) and MoD FIT software (version 3.0; BD Biosciences) (20).

Western blotting. Protein samples were extracted from MHCC-97H and Huh7 cells using RIPA buffer supplemented with a mixture of 1% PMSF and 1% phosphatase inhibitors (Beijing Solarbio Science & Technology Co., Ltd.) and the concentration was measured using a BCA Protein Assay kit (Beijing Solarbio Science & Technology Co., Ltd.). Subsequently. 30 μg of total protein was separated by 10% SDS-PAGE and transferred onto a PVDF membrane (Merck KGaA). After blocking with 5% non-fat milk at room temperature for 1 h, the membrane was incubated with primary antibodies at 4˚C overnight, including anti-CDK2 (1:5,000), anti-CDK4 (1:2,000), anti-cyclin A2 (1:5,000), anti-cyclin E1 (1:1,000), anti-p-JNK (1:1,000), anti-JNK (1:1,000), anti-p-p38 (1:1,000), anti-p38 (1:1,000), anti-GADD45α (1:1,000) and anti-GAPDH (1:10,000), followed by incubation with horseradish peroxidase (HRP)-conjugated Goat Anti-Rabbit IgG (1:10,000; cat. no. SA00001-2, Proteintech Group, Inc.) or HRP-conjugated Goat Anti-Mouse IgG (1:10,000; cat. no. SA00001-1, Proteintech Group, Inc.) secondary antibodies at room temperature for 1 h. The signal was developed with an enhanced chemiluminescence reagent (New Cell & Molecular Biotechnology Co., Ltd.), and images were captured using an Amersham ImageQuant 800 imaging system (Cytiva). The quantification of protein abundance was performed using ImageJ software (version 1.51; National Institutes of Health), with GAPDH as an endogenous control.

Plasmid construction and cell transfection. GADD45α knockdown plasmids containing pPLK GFP+Puro plasmid backbone [short hairpin (sh)-negative control (NC) and shGADD45α, pPLK GFP+Puro], were provided by Beijing Tsingke Biotech Co., Ltd. The 2nd generation system was used for plasmid packaging. A total of 1.5 μg knockdown plasmids, 1 μg pCMV-VSV-G and 0.5 μg pCAG-dR8.9 (packaging plasmid provided by Beyotime Institute of Biotechnology) were transfected into 293T cells in 6-well plates using Lipofectamine 3000® transfection reagent (Thermo Fisher Scientific, Inc.) according to the manufacturer's instructions at 37˚C. Lentiviral particles were harvested at 48 h after transfection, followed by infection of HCC cells for 24 h and screening of the cells for 7 days with medium containing 2 μg/ml puromycin (Beyotime Institute of Biotechnology). The target sequences of the knockdown lentiviral plasmids were as follows: shNC, 5'-TGTCGCGGTAAGTGCCTCATA-3'; GADD45α sh1, 5'-GCTGGAGAGCAGAAGACCGAA-3'; GADD45α sh2, 5'-GAAGACCGAAAGGATGGATAA-3'; and GADD45α sh3, 5'-CAATGGGTTCCAGTGATTAAT-3'.

In vivo studies. A total of 12 four-week-old female BALB/c nude mice (weight, 15-16 g) were purchased from Beijing Vital River Laboratory Animal Technology Co., Ltd. and housed in the animal facility under standard conditions with a controlled temperature of 25±2˚C, a humidity of 55±5%, a light/dark photoperiod of 12 h and free access to water and food. The study was conducted in compliance with the 'Animal Research: Reporting of *In Vivo* Experiments' guidelines. Animal experiments were approved by the Animal Care and Use Committee of The First Affiliated Hospital of Zhengzhou University (Zhengzhou, China; approval no. 2023-KY-1008-002). Huh7 cells were collected in the logarithmic growth phase and resuspended in PBS at a density of $5x10^7$ cells/ml. Each mouse received a subcutaneous injection of 100 μl ($5x10^6$) cell suspension into the right flank. The mice were then randomly divided into two groups and treated with DMSO or 4 mg/kg carfilzomib. Carfilzomib (dissolved in DMSO and diluted in PBS) was administered intraperitoneally twice a week. Tumor volume and mouse weight were measured every 3-4 days. Tumor volume was calculated using the following formula: Tumor volume=($width^2$ x length)/2. After 4 weeks of treatment, mice were euthanized by cervical dislocation. Subsequently, the subcutaneous tumors were excised and processed for further experiments (21).

Reverse transcription-quantitative PCR (RT-qPCR). VeZol reagent (cat. no. R411-01; Vazyme Biotech Co., Ltd.) was used to extract RNA from MHCC-97H and Huh7 cells. A NanoDrop 2000 spectrophotometer was used to measure the RNA concentration, and cDNA was synthesized from RT of 1 μg total RNA according to the manufacturer's protocol of the RT kit (cat. no. R233-01; Vazyme Biotech Co., Ltd.). A qPCR machine was used to amplify the cDNA using the SYBR Green qPCR Mix (cat. no. Q711-02; Vazyme Biotech Co., Ltd.). The thermocycling conditions for amplification were as follows: 95˚C for 5 min, followed by 40 cycles at 95˚C for 10 sec, 60˚C for 30 sec and a final step at 95˚C for 15 sec, 60˚C for 60 sec and 95˚C for 15 sec. GAPDH was used as an internal control. Subsequently, the $2^{-\Delta\Delta Cq}$ method was used to analyze the gene expression data (22). Primer sequences were as follows: GADD45α forward (F), 5'-CTGGAGGAA GTGCTCAGCAAAG-3' and reverse (R), 5'-AGAGCCACA TCTCTGTCGTCGT-3'; GADD45β F, 5'-GCCAGGATCGCC TCACAGTGG-3' and R, 5'-GGATTTGCAGGGCGATGT CATC-3'; GADD45γ F, 5'-CGTCTACGAGTCAGCCAAAGT C-3' and R, 5'-CGATGTCGTTCTCGCAGCAGAA-3'; and GAPDH F, 5'-GTCTCCTCTGACTTCAACAGCG-3' and R, 5'-ACCACCCTGTTGCTGTAGCCAA-3'.

RNA sequencing and analysis. Total RNA from Huh7 cells was extracted using VeZol reagent (cat. no. R411-01; Vazyme Biotech Co., Ltd.). Furthermore, a NanoDrop 2000 spectrophotometer was used to determine the purity and quantity of RNA. The RNA 6000 Nano Kit (cat. no. 5067-1511;

Agilent Technologies, Inc.) and an Agilent 2100 Bioanalyzer (Agilent Technologies, Inc.) was used to determine RNA integrity. For each sample, 1 μg of the total RNA was used for RNA-seq library preparation using the VAHTS Universal V6 RNA-seq Library Prep Kit (cat. no. NR604-01; Vazyme Biotech Co., Ltd.) per the manufacturer's instructions. Then mRNA was enriched and purified using VAHTS mRNA Capture Beads (cat. no. N401; Vazyme Biotech Co., Ltd.). The purified mRNA was cut into short fragments using fragmentation buffer and reverse transcribed into cDNA using random primers. Second-strand cDNA was synthesized using DNA polymerase I, RNase H, dNTP and buffer oncluded in the VAHTS Universal V6 RNA-seq Library Prep Kit. After performing end repair and adding poly (A), the cDNA fragments were ligated using VAHTS RNA Adapters (cat. no. N803/N804; Vazyme Biotech Co., Ltd.). The ligation products were enriched via PCR amplification to construct the cDNA library template (NovaSeq 6000 S4 Reagent Kit v2.5; 300 cycles; cat. no. 20028312). The quality of these cDNA libraries was evaluated with the Agilent 2100 Bioanalyzer (Agilent Technologies, Inc.). An Illumina Novaseq 6000 (Illumina Inc.) was used for 150 bp paired-end sequencing. The loading concentration was 4 nM, and the concentration was quantified using the Qubit 3.0 (Thermo Fisher Scientific, Inc.). The sequencing was performed by Shanghai OE Biotech Co., Ltd. DESeq (2012) package (version 1.46.0) was used to identify transcriptome differentially expressed genes (23,24). The Hierarchical clustering analysis, volcano map and Kyoto Encyclopedia of Genes and Genomes (KEGG) analysis were produced using R (https://www.r-project.org/) on the OECloud platform (25,26). To complete these analyses, the plate corresponding to the class volume was selected on the OECloud platform for hierarchical clustering analysis, volcano map and KEGG analyses. Subsequently, the sequenced gene expression data, included in the raw data from the Gene Expression Omnibus database (accession no. GSE284346; https://www.ncbi.nlm.nih.gov/geo/query/acc.cgi?acc=GSE284346) was used for further analysis.

Protein-protein interaction (PPI) network. Search Tool for the Retrieval of Interacting Genes/Proteins (STRING) database (version 11.5; https://version-11-5.string-db.org/) is an online search tool for the analysis of PPIs and functional protein networks, which contains confirmed and predicted direct and indirect PPI biological data. In the present study, GADD45α, P38 and JNK were used as query conditions, and the minimum required interaction score was set to >0.4, which is a medium level of confidence.

Immunofluorescence staining. The xenograft tumor tissue was fixed in 10% formalin for 48 h at room temperature, paraffin-embedded and cut into 5 μm-thick paraffin sections. Tissue sections were incubated at 60˚C for 2 h, deparaffinized through xylene, dehydrated in ethanol gradients and subjected to thermal antigen retrieval as samples were heated to boiling in a microwave oven for 10 min with 0.01 mol/l citrate buffer (pH 6.0). The sections were blocked in 10% goat serum (Wuhan Servicebio Technology Co., Ltd.) for 30 min at room temperature and incubated overnight at 4˚C with proliferating cell nuclear antigen (PCNA) primary antibodies (1:200; cat. no. GB11010; Wuhan Servicebio Technology Co., Ltd.). Subsequently, the sections were incubated with CoraLite594-conjugated Goat Anti-Rabbit IgG fluorescent secondary antibodies (cat. no. SA00013-4; 1:500; Proteintech Group, Inc.) for 1 h at room temperature, counterstained with DAPI for 10 min at room temperature and examined using a fluorescence microscope (27).

Hematoxylin and eosin (H&E) staining. The xenograft tumor tissue was fixed in 10% formalin for 48 h at room temperature, paraffin-embedded and cut into 5 μm-thick paraffin sections. Tissue sections were incubated at 60˚C for 2 h, deparaffinized using xylene for 5 min at room temperature and dehydrated in 5 and 95% ethanol gradient 5 min at room temperature. Then, the sections were soaked in hematoxylin solution for 5 min, rinsed in tap water for 1 min, incubated with 1% hydrochloric acid alcohol solution for 3 sec, rinsed in tap water for 1 min and hematoxylin reblue solution was added for 10 sec. Next, the sections were soaked in eosin solution for 5 min. The sections were dehydrated using 75 and 95% gradient ethanol for 5 min at room temperature, then incubated with xylene for 5 min at room temperature and sealed with neutral gum. Observation and analysis were performed under an inverted light microscope. H&E staining reagent was provided by Wuhan Servicebio Technology Co., Ltd. and all incubations were performed room temperature, unless otherwise stated.

Relationship between GADD45a mRNA expression levels and overall survival. The Kaplan-Meier (KM) plotter (http://kmplot.com/analysis/) can perform survival analysis on >54,000 genes, including mRNA, microRNA and proteins, across 21 tumor types, including liver cancer (28,29). This database consolidates information from the Gene Expression Omnibus (GEO), the Cancer Genome Atlas (TCGA) and European Genome-phenome Archive (EGA), providing gene expression profiles and prognostic details for a wide range of tumors (28,29). The datasets used for liver cancer survival analysis in Kaplan Meier plotter are available at TCGA (https://cancergenome.nih.gov/) and GEO databases (dataset GSE9843 is available in the https://www.ncbi.nlm.nih.gov/geo/query/acc.cgi?acc=GSE9843; dataset GSE20017 is available at https://www.ncbi.nlm.nih.gov/geo/query/acc.cgi?acc=GSE20017) (28). In the present study, the KM plotter was used to evaluate the prognostic value of *GADD45α* in patients with HCC. *GADD45α* was entered into the database and the number-at-risk was displayed under the main panel of the OS. Based on the Kaplan-Meier plotter Online Tool, 322 patients with HCC (follow-up of 60 months) were included in the online database and were divided into two groups (high vs. low expression levels) according to the median expression levels of GADD45α. All possible cut-off values were auto selected. Statistical parameters such as survival plot, hazard ratio and log-rank P-values were obtained from the KM plotter Online Tool.

Statistical analysis. Statistical analysis was performed using SPSS 16.0 (SPSS, Inc.). Data are presented as the mean ± SD. An unpaired Student's t-test was used to compare two groups and one-way ANOVA followed by Tukey's post hoc test was used to compare multiple groups. Kaplan-Meier analysis

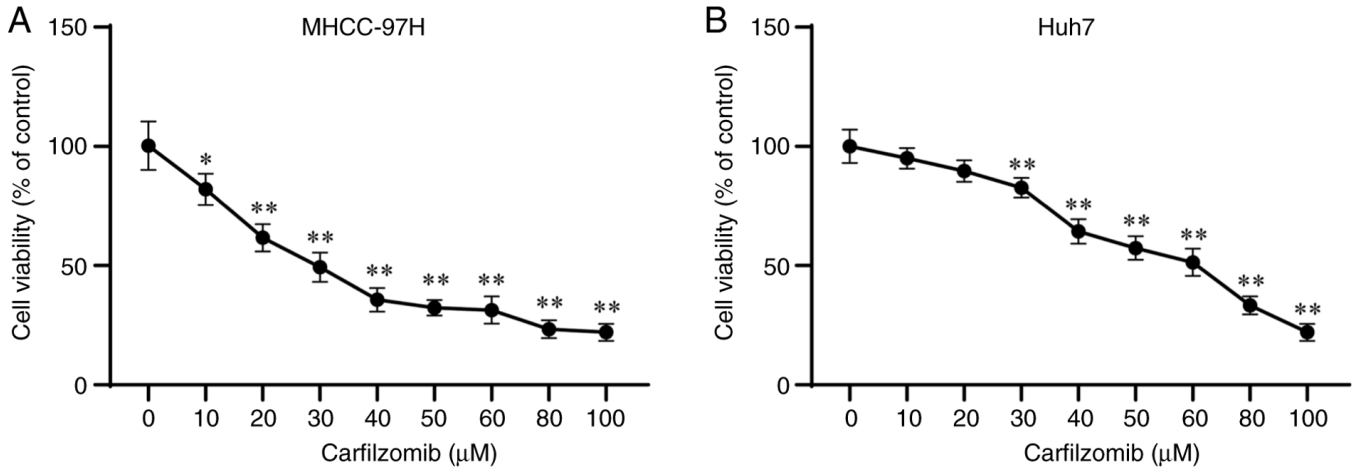

Figure 1. Carfilzomib inhibits the viability of MHCC-97H and Huh7 cells. Cell Counting Kit-8 assay was used to determine the cell viability of (A) MHCC-97H and (B) Huh7 cells treated with several concentrations of carfilzomib for 24 h. Data are presented as the mean ± SD (n=3). *P<0.05 and **P<0.01 vs. 0 μM.

followed by the log-rank test was used to evaluate the prognosis of patients. P<0.05 was considered to indicate a statistically significant difference.

Results

Carfilzomib inhibits the viability of HCC cells. To assess the effect of carfilzomib on HCC cells, MHCC-97H and Huh7 cells were treated with several concentrations of carfilzomib. As shown in Fig. 1A and B, carfilzomib decreased the viability of MHCC-97H and Huh7 cells in a dose-dependent manner. Based on the results of the CCK-8 assay, the activity of MHCC-97H and Huh7 cells decreased by ~50% at carfilzomib concentrations of 30 and 60 μM, carfilzomib concentrations of 30 and 60 μM were used for subsequent experiments on MHCC-97H and Huh7 cells, respectively. These observations collectively suggested that carfilzomib inhibits the viability of HCC cells.

Carfilzomib inhibits HCC cell migration and invasion. The progression of HCC is characterized by the increased motility and invasiveness of cancer cells, which contribute to the high incidence and mortality rate of patients with HCC (30). Therefore, a series of experiments were performed to investigate the effect of carfilzomib on the migration and invasion of HCC cells. The results of the wound-healing assay showed that carfilzomib inhibited the migration of MHCC-97H and Huh7 cells compared with that of the control group (Fig. 2A and B). Transwell assays with (for invasion) or without (for migration) Matrigel were used to corroborate the role of carfilzomib in the migration and invasion of HCC cells. As shown in Fig. 2C and D, carfilzomib significantly suppressed both invasion and migration in MHCC-97H and Huh7 cells compared with those of the control groups. These findings indicated that carfilzomib exhibits strong anti-migratory and anti-invasive properties against HCC cells.

Carfilzomib induces cell cycle arrest in HCC cells. Uncontrolled cell proliferation caused by cell cycle dysregulation is a fundamental feature of cancer cells (31,32). To investigate the anti-proliferative effect of carfilzomib, MHCC-97H and Huh7 cells were treated with carfilzomib, and EdU-staining and colony formation assays were performed. The EdU proliferation assay demonstrated that carfilzomib significantly decreased the number of EdU-positive MHCC-97H and Huh7 cells (Fig. 3A). Consistent with these findings, the colony formation experiments showed that carfilzomib inhibited colony formation in HCC cells compared with that in the control group (Fig. 3B).

To investigate the antiproliferative mechanism of carfilzomib, cell cycle analysis was performed. The results revealed that carfilzomib increased the percentage of cells in the G_0/G_1 phase compared with that in the control group, indicating that carfilzomib caused cell cycle arrest at the G_0/G_1 phase, which reduced entry into the S and G2 phases, particularly in Huh7 cells (Fig. 3C and D). Additionally, the expression of cycle-associated proteins was examined by western blotting. The results demonstrated that carfilzomib significantly decreased the expression of cyclin A2, cyclin E1, CDK2 and CDK4 (Fig. 3E and F) compared with that in the control group in both cell lines. These results indicated that carfilzomib suppressed cell proliferation by inducing G_0/G_1 phase arrest in HCC cells.

Carfilzomib inhibits the growth of HCC xenograft tumors. To assess the antitumor effect of carfilzomib *in vivo*, a Huh7 xenograft tumor model using nude mice was established. In the present study, nude mice were randomly divided into two groups (n=6 per group), which were treated with vehicle control or carfilzomib for 4 weeks. Tumor volume was measured to evaluate the antitumor efficacy of carfilzomib. Carfilzomib significantly reduced tumor growth, volume and weight compared with that in the control group after 17, 21, 24 and 28 days of treatment (Fig. 4A-C). Notably, there was no significant difference in the body weight of carfilzomib-treated mice compared with the control mice (Fig. 4D). Furthermore, analysis of the xenograft tumor tissues using H&E staining, and PCNA immunofluorescence staining showed that the positive rate of PCNA in the carfilzomib group was significantly lower compared with that in

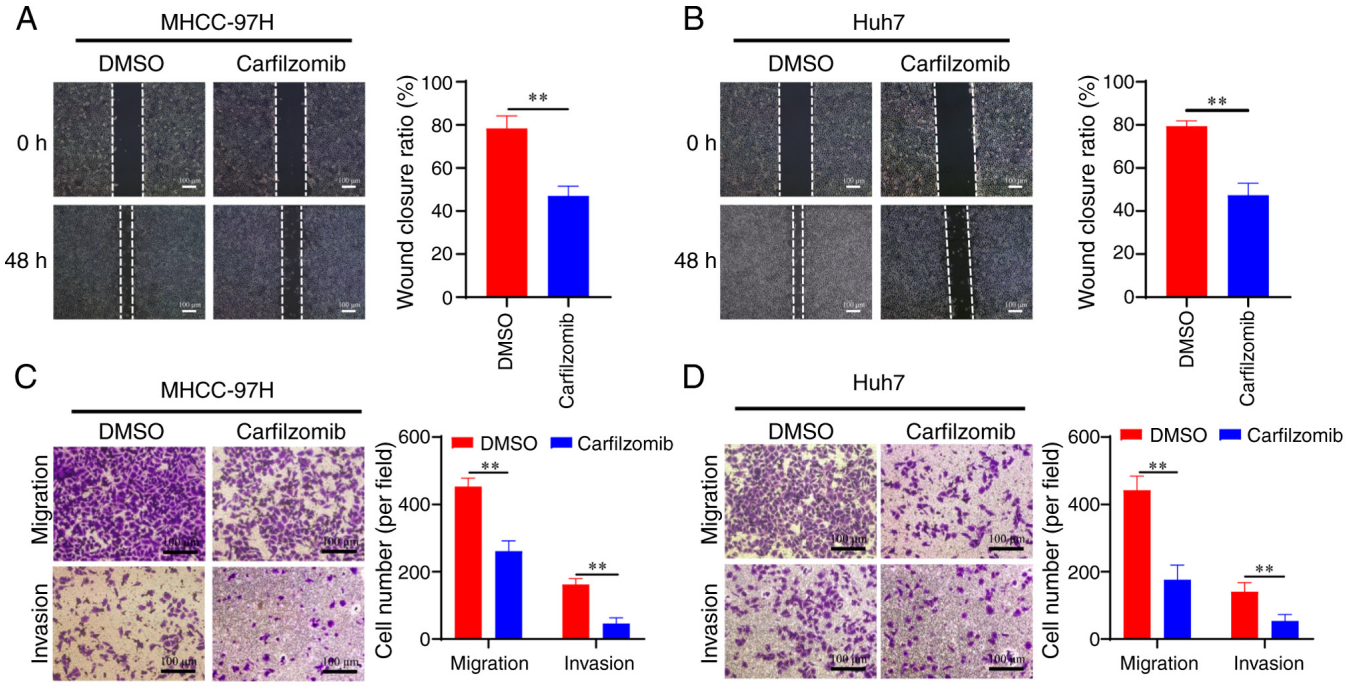

Figure 2. Carfilzomib inhibits migration and invasion in MHCC-97H and Huh7 cells. Migration in (A) MHCC-97H and (B) Huh7 cells after carfilzomib treatment for 24 h was detected by wound healing assay. Migration and invasion were determined using Transwell assays with (for invasion) or without (for migration) Matrigel in (C) MHCC-97H and (D) Huh7 cells. Scale bar, 100 μm. Data are presented as the mean ± SD (n=3). **P<0.01.

the control group (Fig. 4E and F). These findings indicated that carfilzomib significantly inhibited tumor cell proliferation *in vivo*.

Carfilzomib upregulates GADD45α level in HCC cells. To investigate the mechanism of carfilzomib action in HCC cells, transcriptome sequencing was performed in Huh7 cells treated with or without carfilzomib (Fig. 5A and B). The results showed that GADD45α exhibited the highest expression among the most significant top five differentially expressed cell cycle-related genes (Fig. 5C). Carfilzomib also exhibited a significant effect on the expression of GADD45β and GADD45γ (Fig. S1); however, carfilzomib exhibited the most marked effect on GADD45α expression; therefore, in the present study the effect of carfilzomib on GADD45α was investigated. Western blot analysis demonstrated that carfilzomib upregulated the protein expression level of GADD45α (Fig. 5D and E). Simultaneously, analysis of data from The Cancer Genome Atlas showed that higher expression of GADD45α was associated with improved survival of patients with HCC compared with low GADD45α expression (Fig. 5F). These findings indicated that GADD45α may mediate the effects of carfilzomib in HCC cells.

Carfilzomib inhibits cell cycle progression by upregulating GADD45α expression in HCC cells. To investigate the role of GADD45α in the carfilzomib-mediated antitumor effect on HCC, stable GADD45α knockdown cell lines were constructed using lentiviral shRNA targeting GADD45α (Fig. S2). Based on the expression of the GADD45α protein, sh2 was the most effective shRNA tested and was used for the subsequent experiments. The results demonstrated that knockdown of GADD45α counteracted the cell cycle inhibitory effects of carfilzomib on the G_0/G_1 phase (Fig. 6A and B). Furthermore, the EdU proliferation assay showed that carfilzomib decreased the number of positive cells, while silencing GADD45α abolished the anti-proliferative effect of carfilzomib (Fig. 6C and D). Moreover, the expression of proteins involved in cell cycle regulation was examined using western blotting, including cyclin A2, cyclin E1, CDK2 and CDK4. As shown in Fig. 6E and F, silencing GADD45α increased the expression levels of cyclin A2, cyclin E1, CDK2 and CDK4 compared with those in the carfilzomib-treated group. Collectively, these findings indicated that GADD45α serves a crucial role in carfilzomib-mediated antitumor therapy.

GADD45α induces cell cycle arrest by activating MAPK signaling. The MAPK signaling pathway serves a crucial role in cell cycle arrest (33). Kyoto Encyclopedia of Genes and Genomes (KEGG) pathway enrichment analysis indicated significant enrichment of the 'MAPK signaling pathway' with carfilzomib treatment in Huh7 cells (Fig. 7A). STRING network analysis revealed a strong association between GADD45α and proteins involved in the MAPK signaling pathway (Fig. 7B). To assess the role of GADD45α in the MAPK signaling pathway, the expression levels of JNK, p-JNK, p38 and p-p38 were examined using western blotting. As shown in Fig. 7C and D, carfilzomib upregulated the phosphorylation levels of JNK and p38, suggesting that carfilzomib activated the MAPK signaling pathway. Moreover, silencing GADD45α significantly decreased the levels of p-JNK and p-p38 (Fig. 7C and D). These findings indicated that carfilzomib may induce cell cycle arrest in HCC cells via GADD45α-mediated MAPK activation.

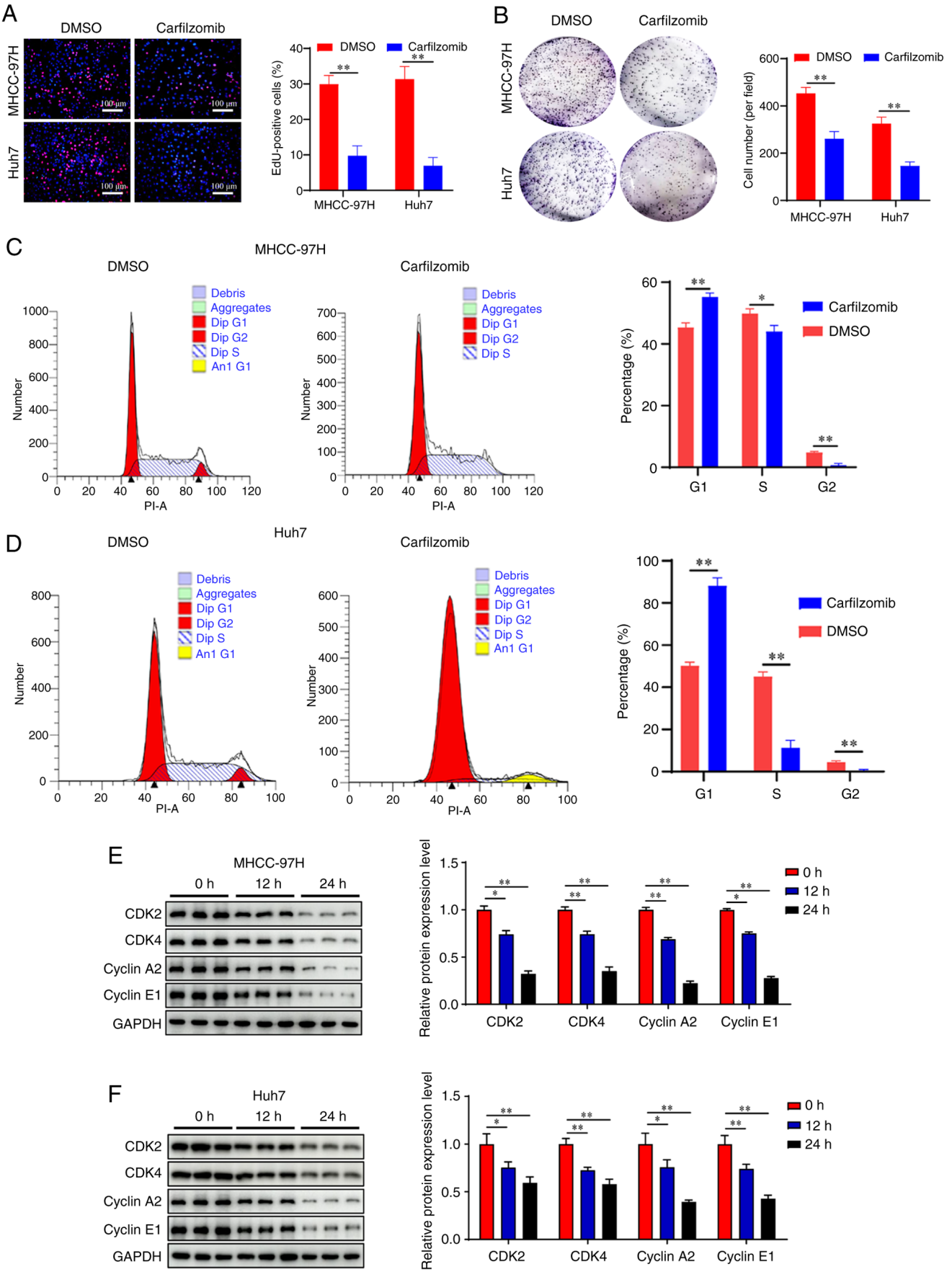

Figure 3. Carfilzomib inhibits the proliferation of MHCC-97H and Huh7 cells. (A) Cell proliferation was assessed using an EdU-staining assay. Scale bar, 100 μm. (B) Representative images and quantification of colony formation assay. The cell cycle distribution of (C) MHCC-97H and (D) Huh7 cells was analyzed by flow cytometry. The expression levels of CDK2, CDK4, cyclin A2 and cyclin E1 were analyzed by western blotting in (E) MHCC-97H and (F) Huh7 cells. GAPDH was used as a loading control. Data are presented as the mean ± SD (n=3). *P<0.05; **P<0.01. CDK, cyclin-dependent kinase; EdU, 5-ethynyl-2-deoxyuridine.

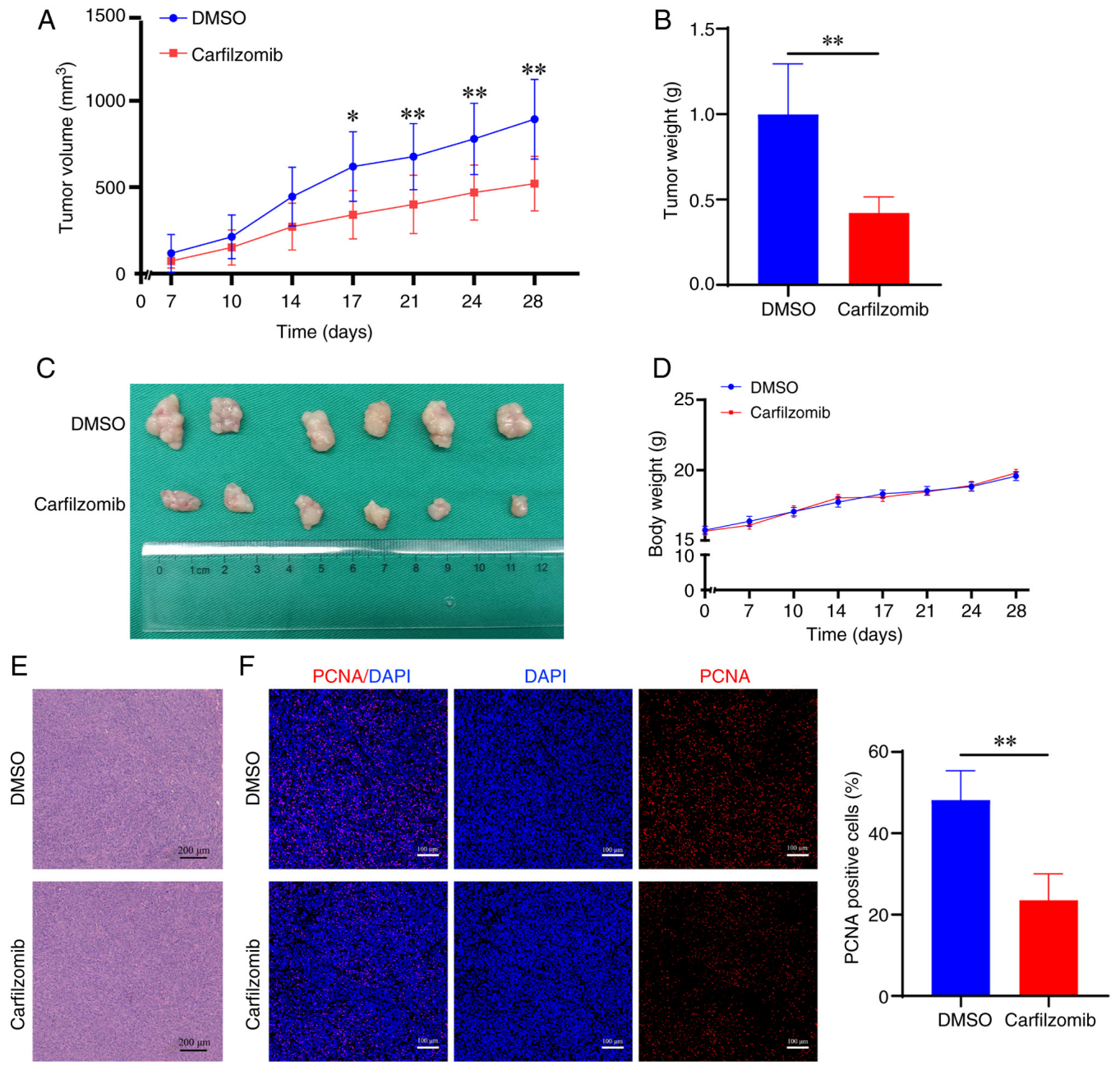

Figure 4. Carfilzomib attenuates hepatocellular carcinoma tumor growth *in vivo*. (A) Xenograft tumors generated from Huh7 cells treated with or without carfilzomib. The growth of xenograft tumors was measured based on the tumor volume. (B) Weights and (C) images of xenograft tumors at the end of the experiment. (D) Body weights of mice in the different treatment groups. (E) H&E staining of xenograft tumor tissues in different treatment groups. (F) Immunofluorescence results for PCNA in xenograft tumor tissues from different treatment groups. Scale bar, 100 μm. Data are presented as the mean ± SD (n=6). *P<0.05, **P<0.01. PCNA, proliferating cell nuclear antigen.

Discussion

Sorafenib was the clinically approved pharmaceutical agent for unresectable HCC prior to the approval of regorafenib (34). However, both sorafenib and regorafenib have demonstrated poor overall survival in certain patients (35,36). The drug discovery approach has proven challenging, particularly in HCC. Carfilzomib is a proteasome inhibitor approved by the Food and Drug Administration for treating multiple myeloma (37). Targeting the proteasome may be a promising approach for treating solid tumors. In a phase I clinical trial, a combination of carfilzomib and irinotecan achieved 20% partial response and 6% stable disease in patients with small cell lung cancer (37). However, the efficacy of carfilzomib in patients with HCC has been poorly studied. The present results indicated that carfilzomib could delay tumor cell proliferation, invasion and migration *in vitro* and *in vivo*, thus establishing carfilzomib as a potential therapeutic agent for HCC.

There is growing consensus that cell cycle dysregulation has long been described as a hallmark and one of the causes of cancer (38). Cyclins, CDKs and CDK inhibitors tightly regulate the cell cycle. CDKs regulate cell cycle events, including initiation, progression and completion of the cell cycle (39). G_1/S phase progression is regulated by the binding

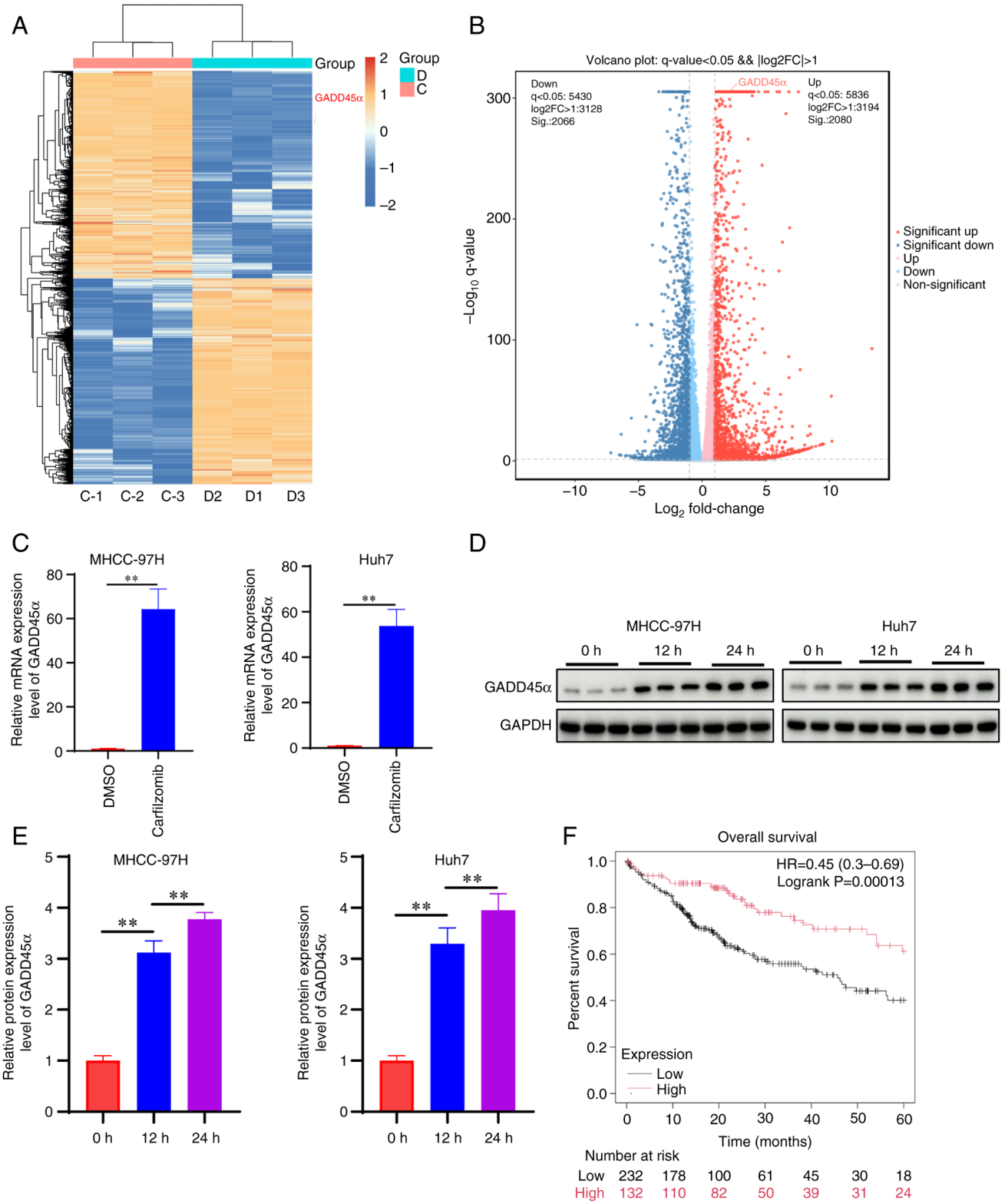

Figure 5. Carfilzomib upregulates the expression of GADD45α in MHCC-97H and Huh7 cells. (A) Hierarchical clustering analysis of the differentially expressed genes in Huh7 cells after treatment with or without carfilzomib. (B) Volcano plot showing differentially expressed genes from transcriptome sequencing. (C) GADD45α mRNA expression levels in MHCC-97H and Huh7 cells detected by reverse transcription-quantitative PCR analysis. (D) Western blotting and (E) semi-quantification of GADD45α expression. (F) KM Plotter Online Tool was used to analyze the overall survival of patients with hepatocellular carcinoma exhibiting high and low levels of GADD45α expression. Data are presented as the mean ± SD (n=3). **P<0.01. GADD45α, growth arrest and DNA damage inducible a; C, carfilzomib; D, DMSO.

of CDKs 4/6 to cyclin D and CDK2 to cyclin E, which eventually phosphorylates the retinoblastoma protein (40). To determine the effect of carfilzomib on cell cycle arrest in HCC cells, cell cycle distribution was analyzed by flow cytometry. The results demonstrated that carfilzomib notably induced cell cycle arrest at the G_0/G_1 phases after 24 h of treatment.

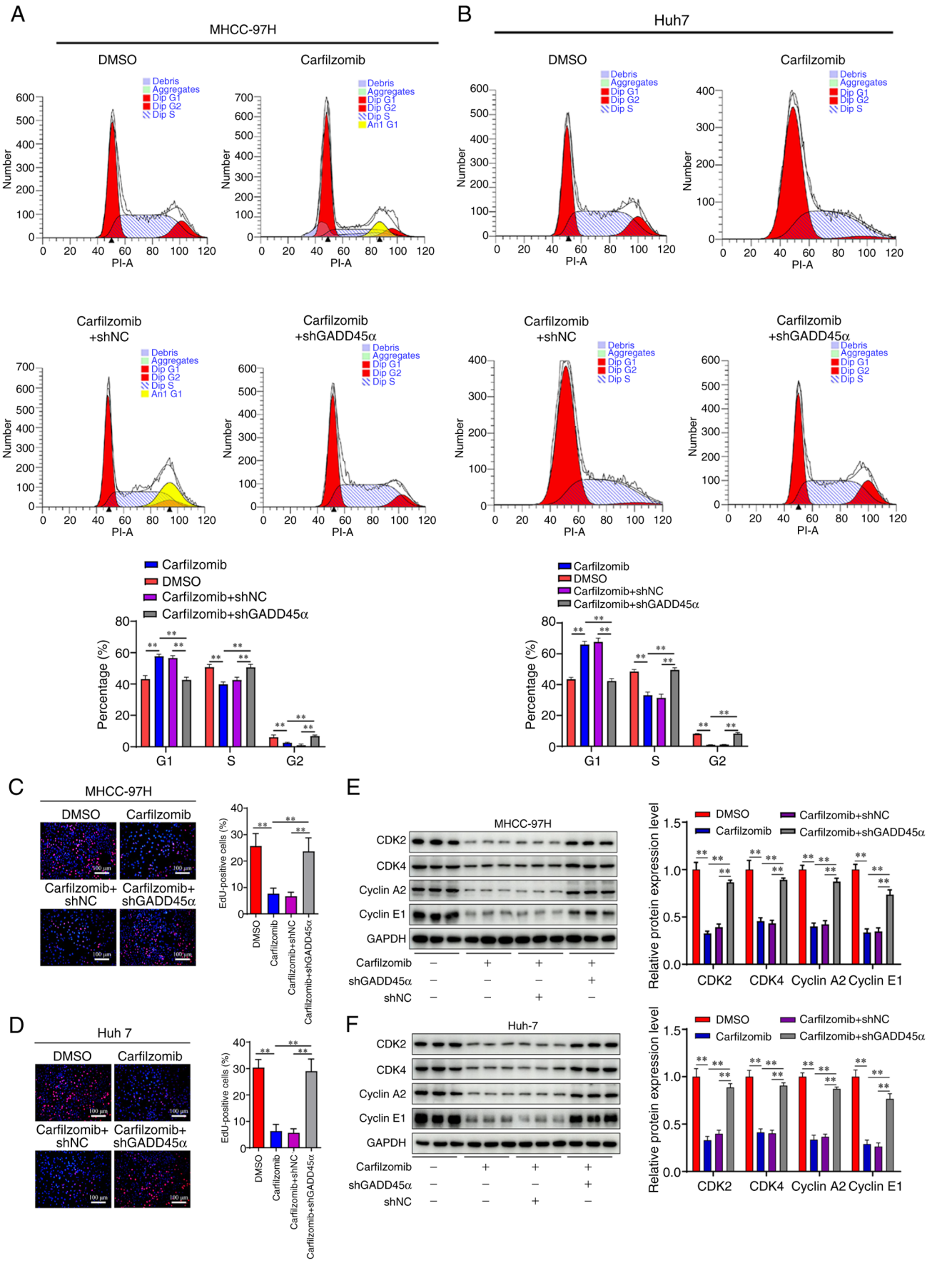

Figure 6. Carfilzomib inhibits the proliferation of MHCC-97H and Huh7 cells by upregulating GADD45α. The cell cycle distribution of (A) MHCC-97H and (B) Huh7 cells was analyzed by flow cytometry. The proliferation of (C) MHCC-97H and (D) Huh7 cells was assessed by the EdU-staining assay. Scale bar, 100 μm. The expression of CDK2, CDK4, cyclin A2 and cyclin E1 was analyzed by western blotting in (E) MHCC-97H and (F) Huh7 cells. Data are presented as the mean ± SD (n=3). **P<0.01. GADD45α, growth arrest and DNA damage inducible α; CDK, cyclin-dependent kinase; EdU, 5-ethynyl-2-deoxyuridine, sh, short hairpin; NC, negative control.

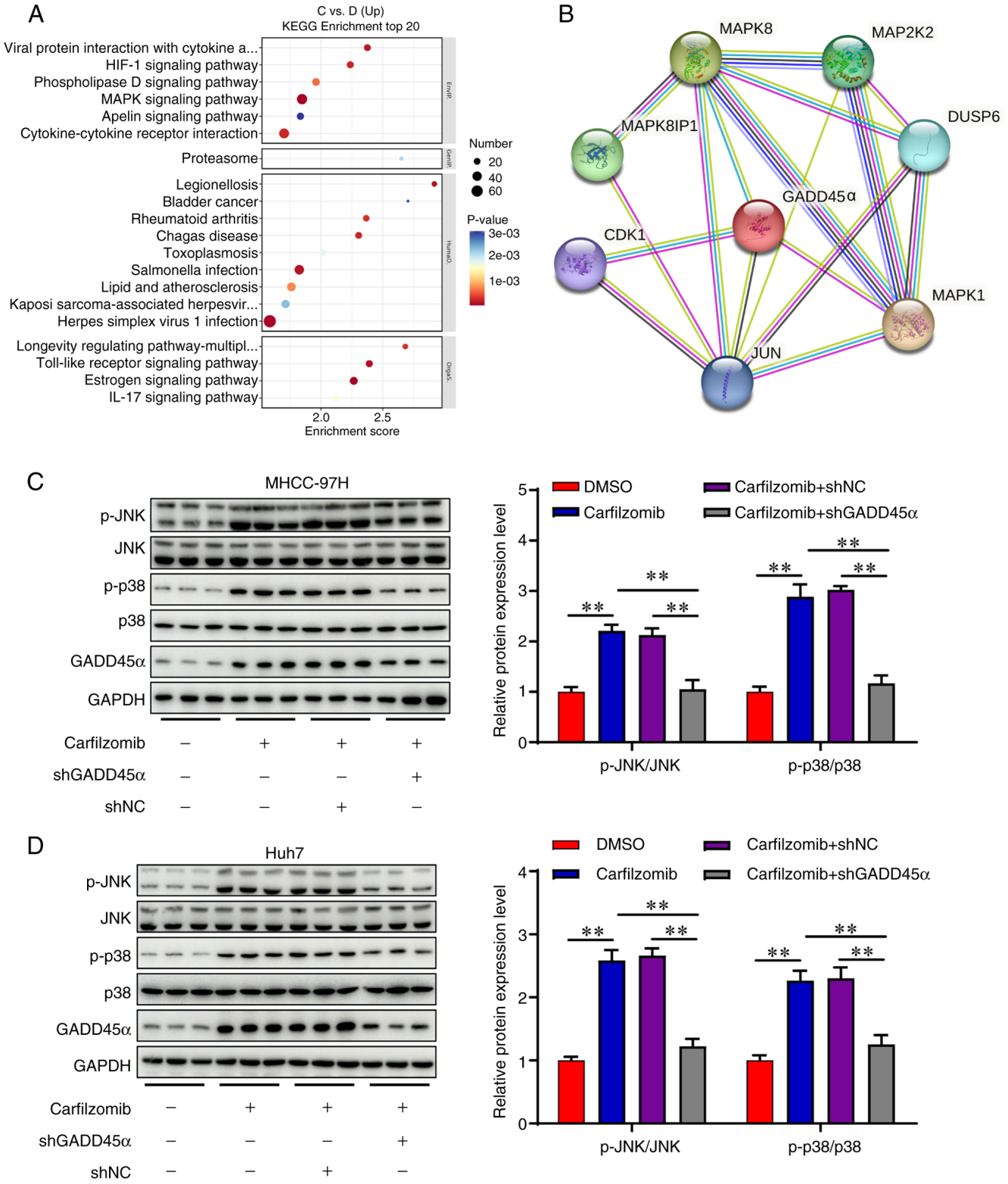

Figure 7. Carfilzomib inhibits cell proliferation by activating the MAPK signaling pathway. (A) KEGG enrichment analysis of the differential expressed genes in Huh7 cells with or without carfilzomib treatment. (B) Functional protein interaction analysis was performed using the STRING database. The protein levels of p-JNK, JNK, p-p38, p38 and GADD45α were analyzed by western blotting in (C) MHCC-97H and (D) Huh7 cells. Data are presented as the mean ± SD (n=3). **P<0.01. MAPK, mitogen-activated protein kinase; GADD45α, growth arrest and DNA damage inducible α; KEGG, Kyoto Encyclopedia of Genes and Genomes; NC, negative control; sh, short hairpin; p, phosphorylated; C, carfilzomib; D, DMSO.

Furthermore, western blot analyses indicated that carfilzomib significantly downregulated the expression of cyclin A2, cyclin E1, CDK2 and CDK4, providing further evidence for the carfilzomib-mediated arrest at the G_0/G_1 phase. These effects suggested a potential mechanism affecting cell cycle regulation in HCC cells in response to carfilzomib treatment.

The cell cycle is regulated by several inhibitory proteins, including the GADD protein family, which prevent

inappropriate mitosis by regulating the cell cycle checkpoints (41). GADDs serve an important role in the DNA damage signal transduction pathway (42). Cell cycle arrest may occur due to carfilzomib activating signal transduction in HCC cells. The present study demonstrated that carfilzomib induced GADD45α expression in HCC cells, which may be associated with cell cycle arrest at the G_0/G_1 phases. Previous studies reported that adenoviral-mediated GADD45α mRNA and protein overexpression led to apoptosis in pancreatic cancer cells by activating caspase-9 and inducing cell cycle arrest (43). Moreover, GADD45α shRNA abolished carfilzomib-mediated cell cycle arrest. Although carfilzomib appears to induce GADD45α expression and cell cycle arrest, the underlying mechanisms remain unclear.

MAPK pathways serve a key role in several cellular processes, including proliferation, differentiation and apoptosis (44). MAPK signaling has been demonstrated to promote GADD45α expression by activating p38 and JNK kinases (45). Specifically, these kinases activate c-Jun, which binds directly to the GADD45α promoter and activates its transcription (46). In a number of cases, GADD45α has been shown to mediate apoptosis via the p38 and JNK pathways (47,48). GADD45α can also bind to the N-terminus of mitogen-activated protein kinase kinase kinase 4 and activate p38 and JNK signaling, which in turn functions as an upstream activator of GADD45α, forming a positive feedback loop that increases the levels of the tumor suppressor protein GADD45α in the event of unresolved DNA damage (49). In addition, GADD45α expression is critical for maintaining p38 and JNK signaling, resulting in keratinocyte growth arrest after UV irradiation (50). In lymphocytes, activation of p38 is essential for apoptosis induced by riboflavin and ultraviolet light, and GADD45α serves a crucial role in modulating this process (51). In the present study, the MAPK signaling pathway was enriched in KEGG pathway analysis following the treatment of Huh7 cells with carfilzomib. In addition, knockdown of GADD45α reduced the activation of the MAPK pathway and abolished the effects of carfilzomib. These data suggested that carfilzomib-mediated cell cycle arrest may be associated with GADD45α-induced activation of the MAPK pathway.

To the best of our knowledge, the present study is the first to explore the possible underlying mechanisms of carfilzomib in HCC. However, the present study has certain limitations. While the effect of carfilzomib on HCC has previously been reported, the present study is an important supplement to highlight the mechanism of carfilzomib in the treatment of HCC. In addition, whether GADD45α inhibits HCC growth in carfilzomib-treated cells by regulating pathways other than MAPK is still unclear and requires further investigation. Moreover, an inducible Cre knockout model of GADD45α would be more physiologically relevant compared with GADD45α knockdown cell lines to study the GADD45α-mediated anti-HCC progression of carfilzomib, which will be addressed in future studies, as lentivirus-mediated GADD45α knockdown still retains a small amount of GADD45α, and this small amount of GADD45α is still functional.

In summary, the present study demonstrated that carfilzomib has marked anticancer effects in HCC cells and exerts its action through the GADD45α-mediated MAPK pathway. Furthermore, the current study provided a theoretical basis for future clinical applications of carfilzomib as a potent chemotherapeutic agent for the treatment of HCC.

Acknowledgements

Not applicable.

Funding

The present study was supported by the Henan Provincial Science and Technology Research Plan (grant no. 222102310534), the Key Scientific Research Project of Henan Higher Education Institutions of China (grant no. 24B320024) and the Foundation of Henan Charity Federation (grant no. GDXZ2023003).

Availability of data and materials

The data generated in the present study may be requested from the corresponding author. The raw sequencing data generated in the present study may be found in the Gene Expression Omnibus database under accession no. GSE284346 or at the following URL: https://www.ncbi.nlm.nih.gov/geo/query/acc.cgi?acc=GSE284346.

Authors' contributions

MC, XC and WG designed the study. MC, XC, YS and CJ performed data acquisition and data analysis. MC and XC drafted the manuscript. MC, YS, CJ and WG edited the manuscript. CJ and WG confirm the authenticity of all the raw data. All authors read and approved the final version of the manuscript.

Ethics approval and consent to participate

The animal experiments were approved by the Animal Care and Use Committee of The First Affiliated Hospital of Zhengzhou University (approval no. 2023-KY-1008-002; Zhengzhou, China).

Patient consent for publication

Not applicable.

Competing interests

The authors declare that they have no competing interests.

References

1. Bray F, Laversanne M, Sung H, Ferlay J, Siegel RL, Soerjomataram I and Jemal A: Global cancer statistics 2022: GLOBOCAN estimates of incidence and mortality worldwide for 36 cancers in 185 countries. CA Cancer J Clin 74: 229-263, 2024.
2. Eguia E, Baker T and Baker M: Hepatocellular carcinoma: Surgical management and evolving therapies. Cancer Treat Res 192: 185-206, 2024.
3. Wang H and Li W: Recent update on comprehensive therapy for advanced hepatocellular carcinoma. World J Gastrointest Oncol 13: 845-855, 2021.
4. Peng TR, Weng YF, Wu TW, Wu CC, Chou YC and Hsu CS: Efficacy and safety of sorafenib or lenvatinib for advanced hepatocellular carcinoma after failure of first-line atezolizumab plus bevacizumab: A systematic review and meta-analysis. Cancers (Basel) 16: 2813, 2024.

5. Luo X, He X, Zhang X, Zhao X, Zhang Y, Shi Y and Hua S: Hepatocellular carcinoma: Signaling pathways, targeted therapy, and immunotherapy. MedComm (2020) 5: e474, 2024.
6. Childs A, Aidoo-Micah G, Maini MK and Meyer T: Immunotherapy for hepatocellular carcinoma. JHEP Rep 6: 101130, 2024.
7. Zhang C, Kuo JC, Huang Y, Hu Y, Deng L, Yung BC, Zhao X, Zhang Z, Pan J, Ma Y and Lee RJ: Optimized liposomal delivery of bortezomib for advancing treatment of multiple myeloma. Pharmaceutics 15: 2674, 2023.
8. Wahl K, Siegemund M, Lehner F, Vondran F, Nüssler A, Länger F, Krech T, Kontermann R, Manns MP, Schulze-Osthoff K, *et al*: Increased apoptosis induction in hepatocellular carcinoma by a novel tumor-targeted TRAIL fusion protein combined with bortezomib. Hepatology 57: 625-636, 2013.
9. Alwahsh M, Farhat J, Talhouni S, Hamadneh L and Hergenröder R: Bortezomib advanced mechanisms of action in multiple myeloma, solid and liquid tumors along with its novel therapeutic applications. EXCLI J 22: 146-168, 2023.
10. Lara PN Jr, Longmate J, Reckamp K, Gitlitz B, Argiris A, Ramalingam S, Belani CP, Mack PC, Lau DH, Koczywas M, *et al*: Randomized phase II trial of concurrent versus sequential bortezomib plus docetaxel in advanced non-small-cell lung cancer: A California cancer consortium trial. Clin Lung Cancer 12: 33-37, 2011.
11. Chen KF, Yu HC, Liu TH, Lee SS, Chen PJ and Cheng AL: Synergistic interactions between sorafenib and bortezomib in hepatocellular carcinoma involve PP2A-dependent Akt inactivation. J Hepatol 52: 88-95, 2010.
12. Honma Y, Shimizu S, Takehara T and Harada M: Sorafenib enhances proteasome inhibitor-induced cell death via inactivation of Akt and stress-activated protein kinases. J Gastroenterol 49: 517-526, 2014.
13. Tan CRC, Abdul-Majeed S, Cael B and Barta SK: Clinical pharmacokinetics and pharmacodynamics of bortezomib. Clin Pharmacokinet 58: 157-168, 2018.
14. Dimopoulos MA, Moreau P, Palumbo A, Joshua D, Pour L, Hájek R, Facon T, Ludwig H, Oriol A, Goldschmidt H, *et al*: Carfilzomib and dexamethasone versus bortezomib and dexamethasone for patients with relapsed or refractory multiple myeloma (ENDEAVOR): A randomised, phase 3, open-label, multicentre study. Lancet Oncol 17: 27-38, 2016.
15. Mansour MA, Aljoufi MA, Al-Hosaini K, Al-Rikabi AC and Nagi MN: Possible role of selective, irreversible, proteasome inhibitor (carfilzomib) in the treatment of rat hepatocellular carcinoma. Chem Biol Interact 215: 17-24, 2014.
16. Hu B, Gao J, Shi J, Wen P, Guo W and Zhang S: m^6A reader YTHDF3 triggers the progression of hepatocellular carcinoma through the YTHDF3/m^6 A-EGFR/STAT3 axis and EMT. Mol Carcinog 62: 1599-1614, 2023.
17. Jiang M, Qi F, Zhang K, Zhang X, Ma J, Xia S, Chen L, Yu Z, Chen J and Chen D: MARCKSL1-2 reverses docetaxel-resistance of lung adenocarcinoma cells by recruiting SUZ12 to suppress HDAC1 and elevate miR-200b. Mol Cancer 21: 150, 2022.
18. Guo D, Zhang M, Wei T, Zhang X, Shi X, Tang H, Ding M, Li J, Zhang S and Guo W: NFKBIZ regulates NFκB signaling pathway to mediate tumorigenesis and metastasis of hepatocellular carcinoma by direct interaction with TRIM16. Cell Mol Life Sci 81: 167, 2024.
19. Zhang F, Gao J, Liu X, Sun Y, Liu L, Hu B, Wang Z, Shi J, Guo W and Zhang S: LATS-regulated nuclear-cytoplasmic translocation of SREBP2 inhibits hepatocellular carcinoma cell migration and invasion via epithelial-mesenchymal transition. Mol Carcinog 62: 963-974, 2023.
20. Ding L, Ren C, Yang L, Wu Z, Li F, Jiang D, Zhu Y and Lu J: OSU-03012 disrupts Akt signaling and prevents endometrial carcinoma progression in vitro and in vivo. Drug Des Devel Ther 15: 1797-1810, 2021.
21. Gao J, Shi X, Sun Y, Liu X, Zhang F, Shi C, Yu X, Yan Z, Liu L, Yu S, *et al*: Deficiency of betaine-homocysteine methyltransferase activates glucose-6-phosphate dehydrogenase (G6PD) by decreasing arginine methylation of G6PD in hepatocellular carcinogenesis. Sci China Life Sci 67: 1648-1665, 2024.
22. Livak KJ and Schmittgen TD: Analysis of relative gene expression data using real-time quantitative PCR and the 2(-Delta Delta C(T)) method. Methods 25: 402-408, 2001.
23. Roberts A, Trapnell C, Donaghey J, Rinn JL and Pachter L: Improving RNA-Seq expression estimates by correcting for fragment bias. Genome Biol 12: R22, 2011.
24. Chen S, Zhou Y, Chen Y and Gu J: fastp: An ultra-fast all-in-one FASTQ preprocessor. Bioinformatics 34: i884-i890, 2018.
25. Guo N, Xia Y, He N, Cheng H, Zhang L and Liu J: IRGM deficiency exacerbates sepsis-induced acute lung injury by inhibiting autophagy through the AKT/mTOR signaling pathway. J Inflamm Res 17: 10255-10272, 2024.
26. Wang X, Kuang J, Li XT, Hu X, Liu YH, Hu CP, Wang M, Wang Q and Zhang Z: Dimethyl fumarate is repurposed to ameliorate aortic aneurysm and dissection in mice. Eur J Pharmacol 988: 177215, 2025.
27. Yu Q, Zhang J, Li J, Song Y, Pan J, Mei C, Cui M, He Q, Wang H, Li H, *et al*: Sirtuin 5-mediated desuccinylation of ALDH2 alleviates mitochondrial oxidative stress following acetaminophen-induced acute liver injury. Adv Sci (Weinh) 11: e2402710, 2024.
28. Menyhárt O, Nagy Á and Győrffy B: Determining consistent prognostic biomarkers of overall survival and vascular invasion in hepatocellular carcinoma. R Soc Open Sci 5: 181006, 2018.
29. Győrffy B: Integrated analysis of public datasets for the discovery and validation of survival-associated genes in solid tumors. Innovation (Camb) 5: 100625, 2024.
30. Lin Y, Zhong W, Lin Q, Ye Y, Li S, Chen H, Liu H, Xu L, Zhuang W, Chen S, *et al*: SFPQ promotes the proliferation, migration and invasion of hepatocellular carcinoma cells and is associated with poor prognosis. Am J Cancer Res 13: 2269-2284, 2023.
31. Oshima J and Campisi J: Fundamentals of cell proliferation: Control of the cell cycle. J Dairy Sci 74: 2778-2787, 1991.
32. Evan GI and Vousden KH: Proliferation, cell cycle and apoptosis in cancer. Nature 411: 342-348, 2001.
33. Deng Y, Li Y, Yang M, Gao Y, Luo X, Chen H, Guo M, Yang X, Liu Y, He J, *et al*: Carfilzomib activates ER stress and JNK/p38 MAPK signaling to promote apoptosis in hepatocellular carcinoma cells. Acta Biochim Biophys Sin (Shanghai) 56: 697-708, 2024.
34. Tang W, Chen Z, Zhang W, Cheng Y, Zhang B, Wu F, Wang Q, Wang S, Rong D, Reiter FP, *et al*: The mechanisms of sorafenib resistance in hepatocellular carcinoma: Theoretical basis and therapeutic aspects. Signal Transduct Target Ther 5: 87, 2020.
35. Lv Z, Liu L, You J, Zhou P, Su Y, Zhao K, Zhang J and Zhu F: Small HBV surface antigen drives regorafenib resistance in HCC via KIAA1429-dependent m6A modification of CCR9. J Med Virol 96: e29894, 2024.
36. Leowattana W, Leowattana T and Leowattana P: Systemic treatment for unresectable hepatocellular carcinoma. World J Gastroenterol 29: 1551-1568, 2023.
37. Arnold SM, Chansky K, Leggas M, Thompson MA, Villano JL, Hamm J, Sanborn RE, Weiss GJ, Chatta G and Baggstrom MQ: Phase 1b trial of proteasome inhibitor carfilzomib with irinotecan in lung cancer and other irinotecan-sensitive malignancies that have progressed on prior therapy (Onyx IST reference number: CAR-IST-553). Invest New Drugs 35: 608-615, 2017.
38. Wu H, Li L, Ai Z, Yin J and Chen L: Pristimerin induces apoptosis of oral squamous cell carcinoma cells via G_1 phase arrest and MAPK/Erk1/2 and Akt signaling inhibition. Oncol Lett 17: 3017-3025, 2019.
39. Wang B, Li R, Wu S, Liu X, Ren J, Li J, Bi K, Wang Y and Jia H: Breast cancer resistance to cyclin-dependent kinases 4/6 inhibitors: Intricacy of the molecular mechanisms. Front Oncol 11: 651541, 2021.
40. Desvoyes B and Gutierrez C: Roles of plant retinoblastoma protein: Cell cycle and beyond. EMBO J 39: e105802, 2020.
41. Humayun A and Fornace AJ Jr: GADD45 in stress signaling, cell cycle control, and apoptosis. Adv Exp Med Biol 1360: 1-22 2022.
42. Palomer X, Salvador JM, Griñán-Ferré C, Barroso E, Pallàs M and Vázquez-Carrera M: GADD45A: With or without you. Med Res Rev 44: 1375-1403, 2024.
43. Li Y, Qian H, Li X, Wang H, Yu J, Liu Y, Zhang X, Liang X, Fu M, Zhan Q and Lin C: Adenoviral-mediated gene transfer of Gadd45a results in suppression by inducing apoptosis and cell cycle arrest in pancreatic cancer cell. J Gene Med 11: 3-13, 2009.
44. Kim EK and Choi EJ: Pathological roles of MAPK signaling pathways in human diseases. Biochim Biophys Acta 1802: 396-405, 2010.
45. Wang M, Tian B, Shen J, Xu S, Liu C, Guan L, Guo M and Dou J: Bavachin induces apoptosis in colorectal cancer cells through Gadd45a via the MAPK signaling pathway. Chin J Nat Med 21: 36-46, 2023.

46. Wang Y, Gao H, Cao X, Li Z, Kuang Y, Ji Y and Li Y: Role of GADD45A in myocardial ischemia/reperfusion through mediation of the JNK/p38 MAPK and STAT3/VEGF pathways. Int J Mol Med 50: 144, 2022.
47. Wang HH, Chang TY, Lin WC, Wei KC and Shin JW: GADD45A plays a protective role against temozolomide treatment in glioblastoma cells. Sci Rep 7: 8814, 2017.
48. Peretz G, Bakhrat A and Abdu U: Expression of the Drosophila melanogaster GADD45 homolog (CG11086) affects egg asymmetric development that is mediated by the c-Jun N-terminal kinase pathway. Genetics 177: 1691-1702, 2007.
49. Geifman-Holtzman O, Xiong Y and Holtzman EJ: Gadd45 stress sensors in preeclampsia. Adv Exp Med Biol 793: 121-129, 2013.
50. Hildesheim J, Bulavin DV, Anver MR, Alvord WG, Hollander MC, Vardanian L and Fornace AJ Jr: Gadd45a protects against UV irradiation-induced skin tumors, and promotes apoptosis and stress signaling via MAPK and p53. Cancer Res 62: 7305-7315, 2002.
51. Yang P, Wen H, Zhong T, Hu H, Zhu B, Xia K, Xu M and Bian M: GADD45α is involved in the apoptosis of lymphocytes induced by riboflavin and ultraviolet light. Transfusion 57: 646-656, 2017.